

# Thermo-mechanical approach to validation of deep crustal and lithospheric structures inferred from multidisciplinary data: application to the Western and Northern Alps

E. Burov<sup>1</sup>\*, Y. Podladchikov<sup>2</sup>, G. Grandjean<sup>1</sup> and J. P. Burg<sup>2</sup>

<sup>1</sup>*Direction de la Recherche, BRGM, BP 6009, Orléans, France,* <sup>2</sup>*Geologisches Institut, ETH-Zentrum, Sonneggstrasse 5, CH 8092, Zurich, Switzerland*

## ABSTRACT

Current multidisciplinary studies confront the difficult problem of validation and verification of internal compatibility of geophysical and geological data of different nature, quality and origin. Our 'geodynamic' approach exploits the natural interdependence between the data related to different physical properties of geological structures (density, rheology, temperature, stress). Using the latter as input for a thermo-mechanical finite-element model, we can verify whether the inferred properties and geometries (i) are mechanically stable, (ii) require rheologically consistent stresses, strains, realistic

thermal conditions, etc., and (3) will evolve in a geologically realistic way in the future. This 'mechanically balanced' approach is tested on the Alpine orogen (ECORS and NFP20 profiles) in the framework of the GeoFrance 3D programme. The results suggest a number of corrections and adjustments that can be made to existing seismically- and gravity-predicted geometries of structures such as the Ivrea body and those of the depleted subducted crust.

Terra Nova, 11, 124–131, 1999

## Introduction

Extensive multidisciplinary geophysical studies of the deep crustal structure (i.e. BIRPS, COCORP, DEKORP, ECORS, LITHOPROBE, EUROP-ROBE) have greatly improved our knowledge of mountain and basin dynamics. In France, several preliminary cross-sections derived from the ECORS data have given rise to intensive discussions and quite different geological interpretations (e.g. Bois, 1987), and partly inspired the GéoFrance 3D project (1995) aimed at obtaining a decisive, 3D picture of the regional tectonics by combining various geological and geophysical 2D/3D data sources (Ledru *et al.*, 1997).

Seismic data are a major source of information about the crustal and lithospheric structure. Unfortunately, their interpretations are non-unique. For this reason, potential field data (gravity, magnetics) are used to constrain and complete seismically-derived 3D structures. Gravity and seismic velocity anomalies are related to the same source (density anomalies). Thus, a combination of both methods yields far more reliable geological interpretations than those based on a single method (e.g. Bayer *et al.*, 1989; Kissling, 1993; Kis-

sling and Spakman, 1996). However, seismo-gravity models may still provide quite ambiguous solutions (e.g. Kissling, 1993) and additional criteria are needed to eliminate unrealistic solutions and refine the valid ones.

To persist on geological timescales, subsurface density and lithology structures must stay in a thermo-mechanical equilibrium, be it dynamic or static. For example, low-density, weak subsurface crustal inclusions (e.g. granitic) or structures with sharp, steep boundaries cannot be preserved for longer than 5–10 Myr because of gravity-driven stresses (e.g. Burov *et al.*, 1998). In steadily evolving structures, reasonable strain rates, stresses and other physical characteristics conditioned by rock mechanical data and observations (topography/convergence rates, seismicity, gravity, etc.) must also be taken into account. The approach proposed in our study allows for verification of mechanical stability of hypothetical geological structures inferred from multidisciplinary data, and validation of the physical conditions required for this stability. This 'coupled' methodology is based on a thermo-mechanical numerical model in which the multidisciplinary data serve both as input and output parameters. We tested our method on the Alpine part of ECORS-CROP (Nicolas *et al.*, 1990) and NFP20 (Pfiffner *et al.*, 1988) profiles (Fig. 1). The data include cross-sections derived from deep seismic data (Damotte *et al.*, 1990), wide-angle data (Hirn *et al.*, 1989; Thou-

venot *et al.*, 1990) and gravity modelling (Bayer *et al.*, 1989; Rey *et al.*, 1990). Along these cross-sections, the geometry of deep crustal units (e.g. the Ivrea body, deep crustal thrusts, low-velocity zone) is rather well delineated. Yet a number of key details of fine crustal and lithospheric structure remain poorly constrained allowing for various, noticeably differing, geometrical interpretations (e.g. (Kissling, 1993, fig. 2).

## Geophysical data

Profiles across Western (ECORS) and Northern Alps (NFP20) (Figs 1 and 2) from the ECORS-CROP (Nicolas *et al.*, 1990) and NFP20 (Pfiffner *et al.*, 1988) programmes were derived using seismic cross-sections, gravity profiles, and partly magnetic, geodetic, thermal and stratigraphy data. Seismic data on bulk crustal structure (Damotte *et al.*, 1990; Valasek *et al.*, 1990) and major velocity anomalies (Thouvenot *et al.*, 1990) were converted into density anomalies used in forward gravity models (Rey *et al.*, 1990) to adjust the geometry of the inferred structures. Nevertheless, the ambiguities of seismic imagery and potential field data analysis still allow for various possible interpretations (Fig. 2).

## Basic geophysical features of the Alpine part of the ECORS profile

Alpine mountain building during Eurasia–Africa collision was accompanied

\*Correspondence and Present address: Tectonics Department, University of P. and M. Curie, 75252 Paris, France. E-mail: evgenii.burov@lgs.jussieu.fr

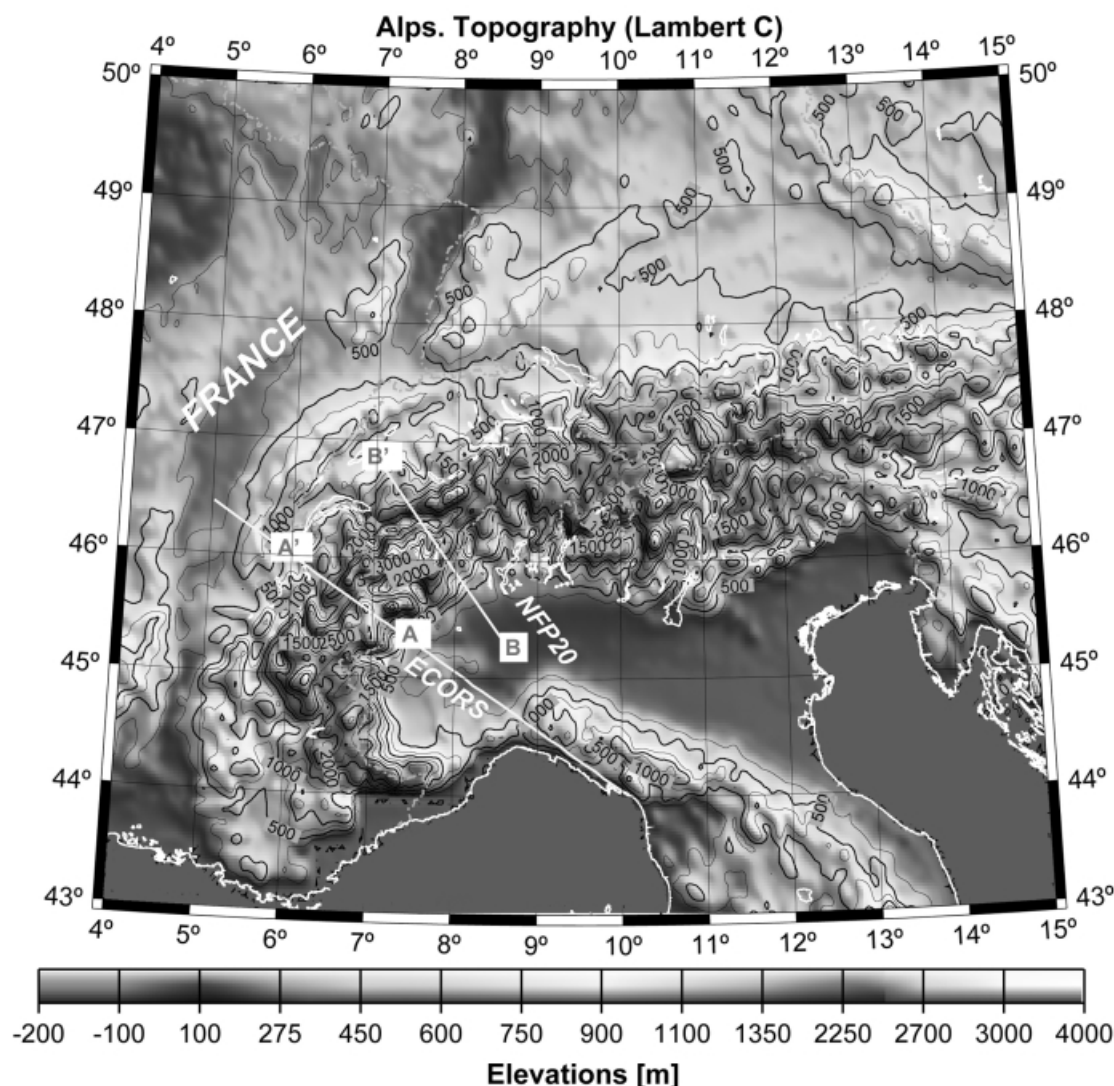


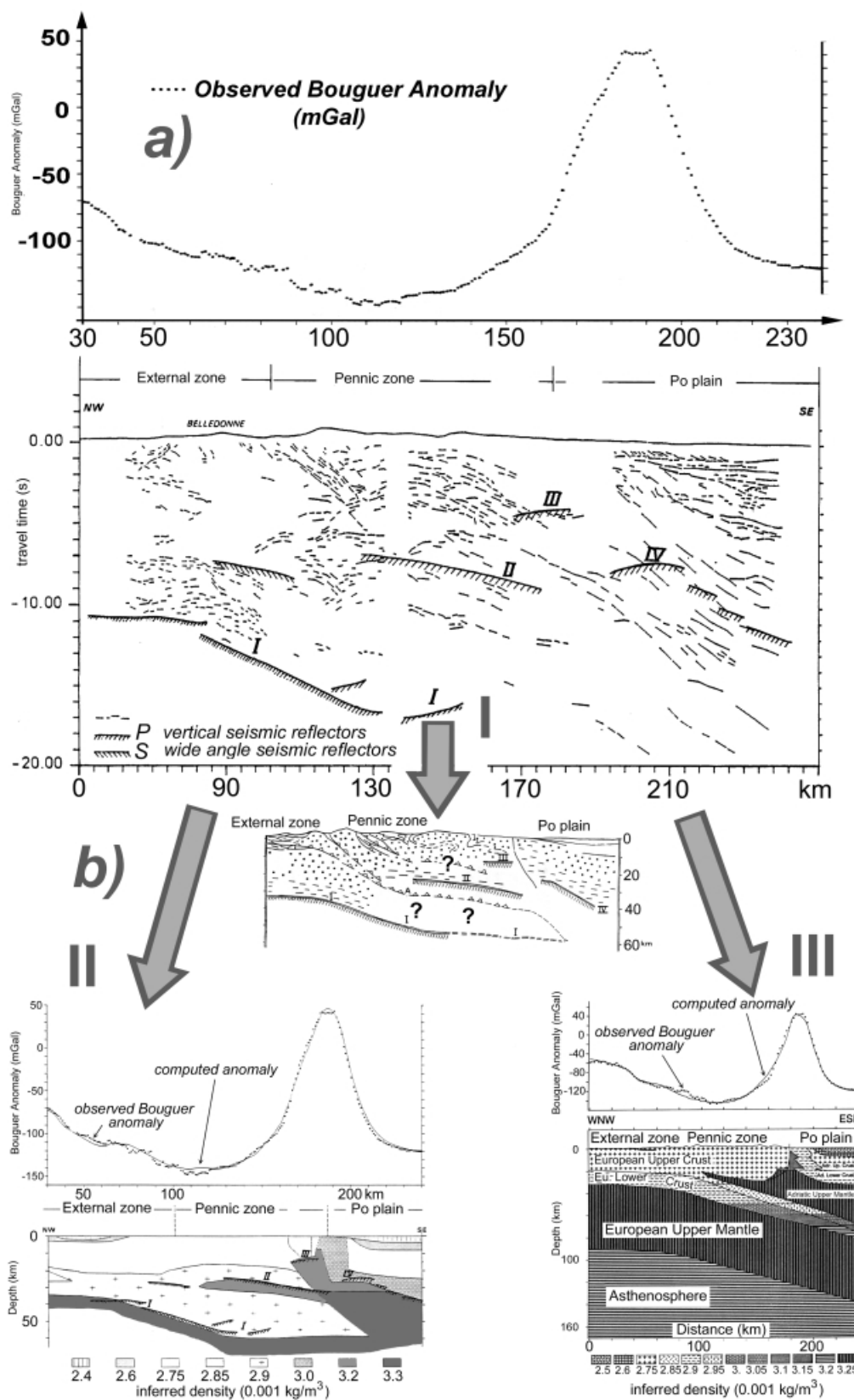
**Fig. 1** Digital topography map (DTM5 5' × 5' data base) of the Alpine belt showing the location of the two test profiles (parts of ECORS and NFP20).

**Fig. 2** (Overleaf, pp. 126–127) Source data (seismic cross-sections, gravity profiles) and previously inferred interpretations (density/lithology structures). (a) unmigrated cross-section of the Alpine part of the ECORS profile and Bouguer gravity profile (ECORS-CROP Deep Seismic Working group, 1989). Wide-angle reflectors I, II, III, and IV are shown. (b) I, primary inferred seismo/gravity consistent structure (from ECORS-CROP Deep Seismic Working group, 1989): I, upper mantle; II, lower granulite crust; III, upper crust; white areas are Mesozoic to Cainozoic covers and Tertiary molasses. II: seismo/gravity consistent structure proposed by (Bayer *et al.*, 1989) (theoretical gravity anomaly is shown with a solid line). III: seismo/gravity consistent structure from (Marchant and Stampfli, 1997) (theoretical gravity anomaly is shown with a solid line).

by numerous tectonic events from early Tertiary onwards (Bernoulli, 1981; Trümpy, 1985; Frei *et al.*, 1990; Nicolas, 1990; Viallon, 1990). For the Western Alps, the SE-dipping oceanic subduction was supposedly succeeded by progressive subduction of the European lithosphere resulting in formation of the Penninic Thrusts (100–40 Ma), sub-Alpine nappes (40–25 Ma), and of the Jura decollement (Nicolas,

1990). The Alpine part of the ECORS profile starts in the Molassic basin, crosses the Belledune, Vanoise and Gran Paradiso massifs and ends in the Pô plain [Figs 1(A–A') and 2a]. On the profile, main seismic reflectors reveal sedimentary layering of the Molassic basin (I), depict structure of the Penninic nappes in the middle crust (II) and trace the layered lower crust from the eastern part of the section to nearly

below the Penninic front (III). The reflective zone (III) disappears westwards, but several wide-angle reflectors located in the continuity at its base indicate potential extension of the Moho beneath the Gran Paradiso (ECORS-CROP Deep Seismic Sound-ing Group, 1989; Thouvenot *et al.*, 1990). Other mid-crustal reflectors are attributed to lower crustal/upper mantle extrusions equally expressed in the



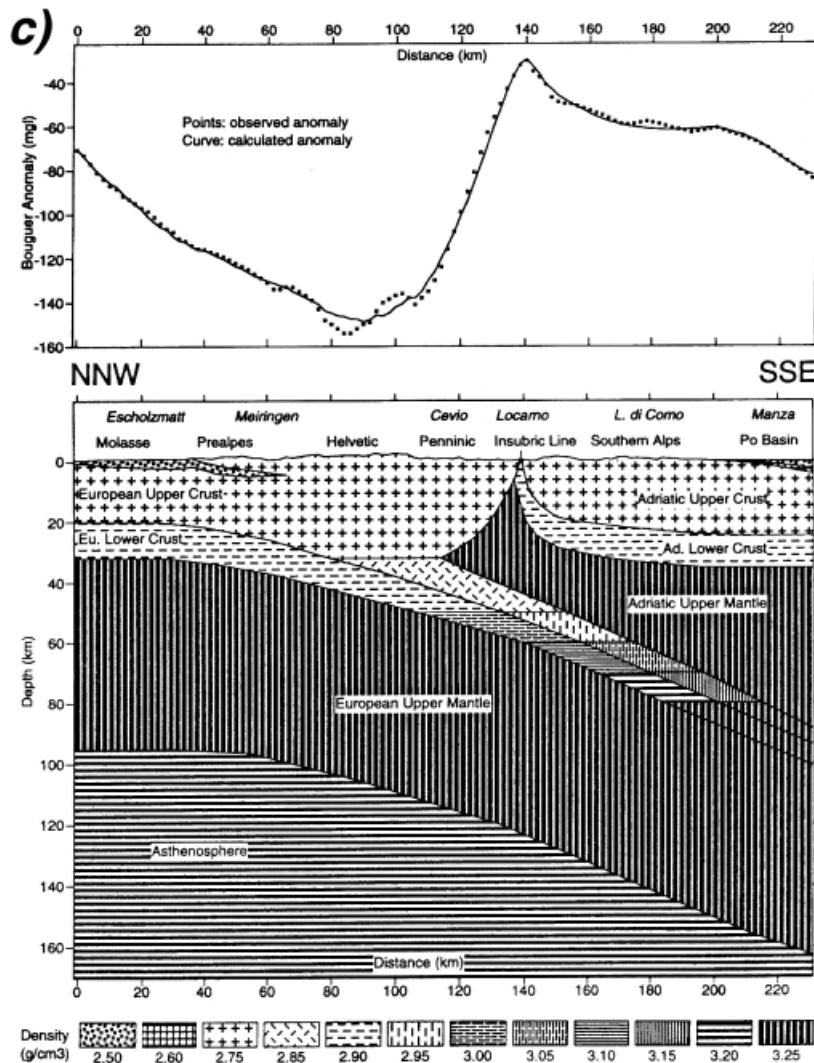
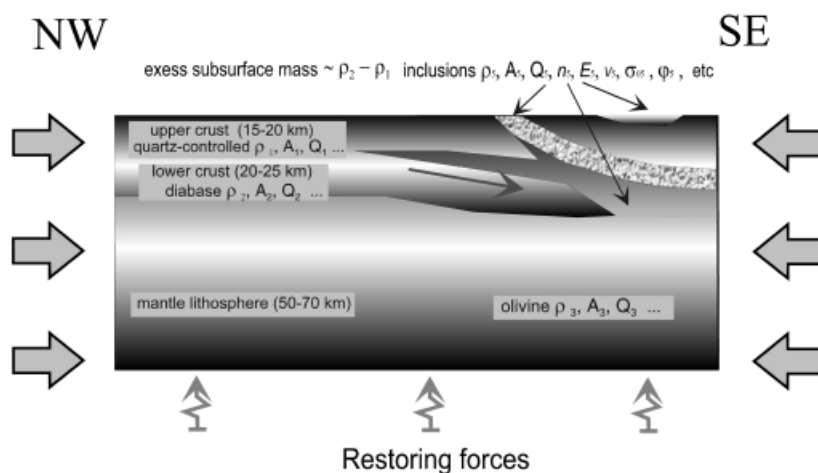


**Fig. 2** (cont.) (c) One of the inferred structures for the Alpine part of the NFP20 profile, observed (dots) and calculated Bouguer gravity anomaly (from Marchant and Stampfli, 1997).



120 mGal Bouguer gravity (Fig. 2) and large magnetic anomaly over the central part of the range. This phenomenon is interpreted as the high-density, high-magnetization lower crustal slab unit named the Ivrea body (e.g. Rey *et al.*, 1990, fig. 2).

### Basic geophysical features of the NFP20-South deep seismic profiles

(Swiss National Science Foundation programme, Figs 1(B–B') and 2c; Frei *et al.*, 1990; Marchant and Stampfli, 1997). The 80 km-long Southern profile begins near the southern rim of the Gotthard massif at the north, crosses the Penninic system to the east of the Lepontine axial culmination, and ends close to the northern rim of the Po basin. It depicts southward-plunging European crust from 35 km to 60 km below the southern Molasse basin and the Central Alpine Zone, respectively. The lower crust is imaged by a gradually deepening reflective zone, while the Moho is underlined by a sharp transition between the reflective crust and transparent upper mantle. Suggested lower crust models refer to the presence of metasediment sequences and mafic intrusions (Frei *et al.*, 1990). The other peculiar feature of this profile is the crustal structure below the base of the Penninic nappes where northward-dipping reflectors depict a protruding wedge, which delaminates the European crust at a mid-crustal level (this is also confirmed by refraction and gravity data (Laubscher, 1988)).

### Model

Our thermo-mechanical model (Fig. 3), derived from the FLAC method (Cundall, 1989; Poliakov *et al.*, 1993), solves equilibrium problems for brittle-elasto-ductile media with spatially varying

**Fig. 3** (Left) Simplified cartoon of the thermo-mechanical finite-element model parameters, mimicking input configuration II from Fig. 2b. Unlimited number of various crustal and lithospheric structures with different material properties ( $\rho_i, A_i, Q_i, n_i, E_i, v_i, \sigma_{0i}, \phi_i$ , see text and Table 1) can be assigned ( $i = 1, 2, 3 \dots n$ , where  $n$  is a number of layers or inclusions, e.g.  $i = 1$  is for the upper crust).

properties, for example, composed of arbitrarily shaped layers, bodies and faults. The material properties are defined through those of the input lithologies, temperature and velocity structure. The algorithm handles strain localizations and can reproduce non-predefined fault distributions comparable with observations. The brittle behaviour is modelled by Mohr–Coulomb plasticity with friction angle  $\phi = 30^\circ$  and cohesion  $\sigma_0 = 20$  MPa. For the elastic part, we use Young modulus  $E = 0.8$  GPa and Poisson's ratio of  $\nu = 0.25$ . (Gerbaut *et al.* 1999). The ductile power law parameters were chosen according to leading lithology (quartz, diabase, olivine and so on, Table 1). The lithosphere rests on a pliable Winkler basement (250 km depth), and undergoes horizontal shortening at  $10 \text{ mm yr}^{-1}$  (for the Alpine zone). The upper surface is free and is formed by the input topography. The numerical mesh counts  $500 \times 250$  rectangular elements composed of overlapping couples of triangular elements (to prevent mesh locking).

We use a fully explicit, time-marching dynamic finite-element scheme solving equations of motion:

$$\rho \partial v_i / \partial t - \partial \sigma_{ij} / \partial x_j - \rho g_i = 0, \quad (1)$$

where  $v$  is velocity,  $g$  is the acceleration due to gravity and  $\rho$  is the density (Fig. 3). Solution of these equations provides velocities at grid points used to calculate element strains  $\varepsilon_{ij}$ , and then, via appropriate constitutive relations, the element stresses  $\sigma_{ij}$  and equivalent forces  $f_i = \rho \partial v_i / \partial t$  forming the input for next calculation cycle. This scheme works practically for any rheology (Cundall, 1989). Strain localizations are handled using an adaptive remeshing technique (Poliakov *et al.*, 1993). The solution of (1) is coupled with the heat transport equation to account for temperature-dependent rheology:

$$\rho C_p \partial T / \partial t - \text{div}(\mathbf{k} \nabla T) + \mathbf{v} \nabla T = H, \quad (2)$$

where  $\mathbf{v}$  is velocity tensor,  $C_p$  is the specific heat,  $\mathbf{k}$  is the thermal conductivity tensor, and  $H$  is heat production per unit volume (we use commonly inferred values — e.g. Burov *et al.*, 1993).

In nature, long-living geological structures should stay in dynamic or static equilibria. If the geometries and properties (density, lithology, etc.) of these structures are inferred incorrectly

**Table 1** Parameters of dislocation creep for lithospheric rocks and minerals. After (Brace and Kohlstedt, 1980; Carter and Tsenn, 1987; Kirby and Kronenberg, 1987; Tsenn and Carter, 1987)

Mineral/rock	$A^* [\text{Pa}^{-n} \text{s}^{-1}]$	$H^* [\text{KJ mol}^{-1}]$	$n$
Quartzite (dry)	$5 \times 10^{-12}$	190	3
	$2.7 \times 10^{-20}$	156	2.4
Diorite (dry)	$5.01 \times 10^{-15}$	212	2.4
	$5.2 \times 10^{-18}$	219	2.4
Diabase (dry)	$6.31 \times 10^{-20}$	276	3.05
	$8.00 \times 10^{-25}$	260	3.4
Olivine/dunite (dry)	$7 \times 10^{-14}$	520	3
Dislocation climb at	$2.5 \times 10^{-17}$	532	3.5

$\sigma_1 - \sigma_3 < 200$  MPa

olivine

(Dorn's dislocation

glide) at

$\sigma_1 - \sigma_3 \geq 200$  MPa)

$$\dot{\varepsilon} = \dot{\varepsilon}_0 \exp \left[ -\frac{H^*}{RT} \left( 1 - \frac{(\sigma_1 - \sigma_3)}{\sigma_0} \right)^2 \right]$$

where  $\dot{\varepsilon}_0 = 5.7 \times 10^{11} \text{ s}^{-1}$ ,  $\sigma_0 = 8.5 \times 10^3$  MPa;  $H^* = 535 \text{ kJ mol}^{-1}$

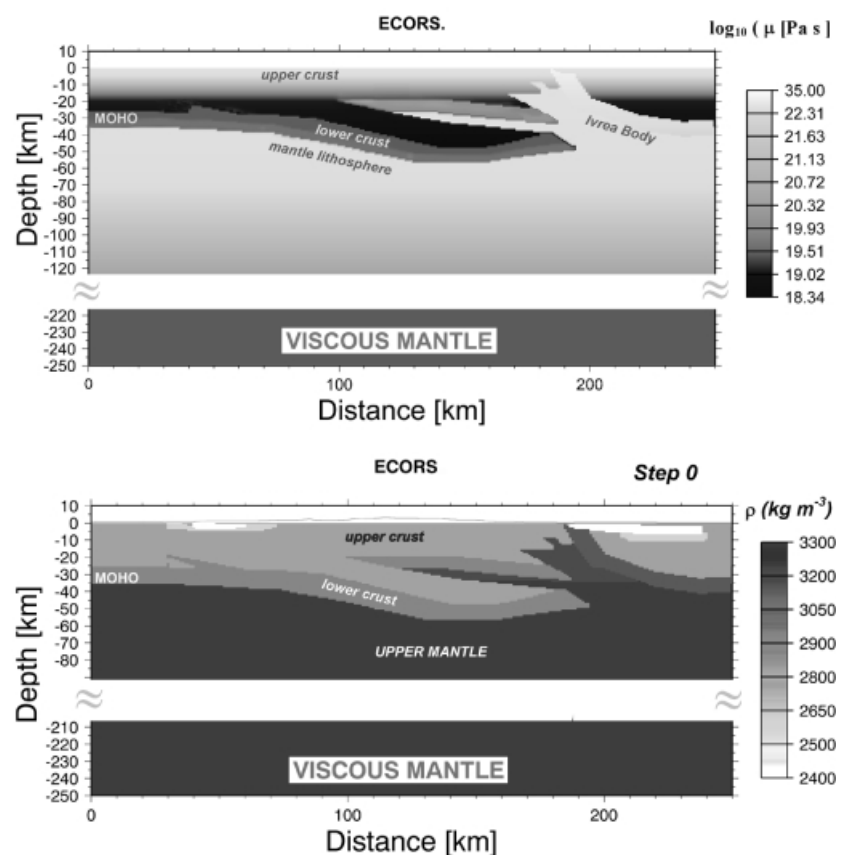


**Fig. 4** Initial viscosity structure for the ECORS profile (top) inferred from the density structure (bottom) and thermal model. The viscosity structure is complemented by plasticity and elasticity structure recomputed on each time step. The rheological phase of each numerical element at given moment of time is defined according to the minimal stress criteria.

(bad interpretation, bad data quality), the mechanical equilibrium model will demonstrate that the inferred structures are mechanically unstable, or imply un-

realistic evolution of the internal structures, velocity and stress distributions (for example, uplift instead of subsidence, too rapid subsidence, etc.). The

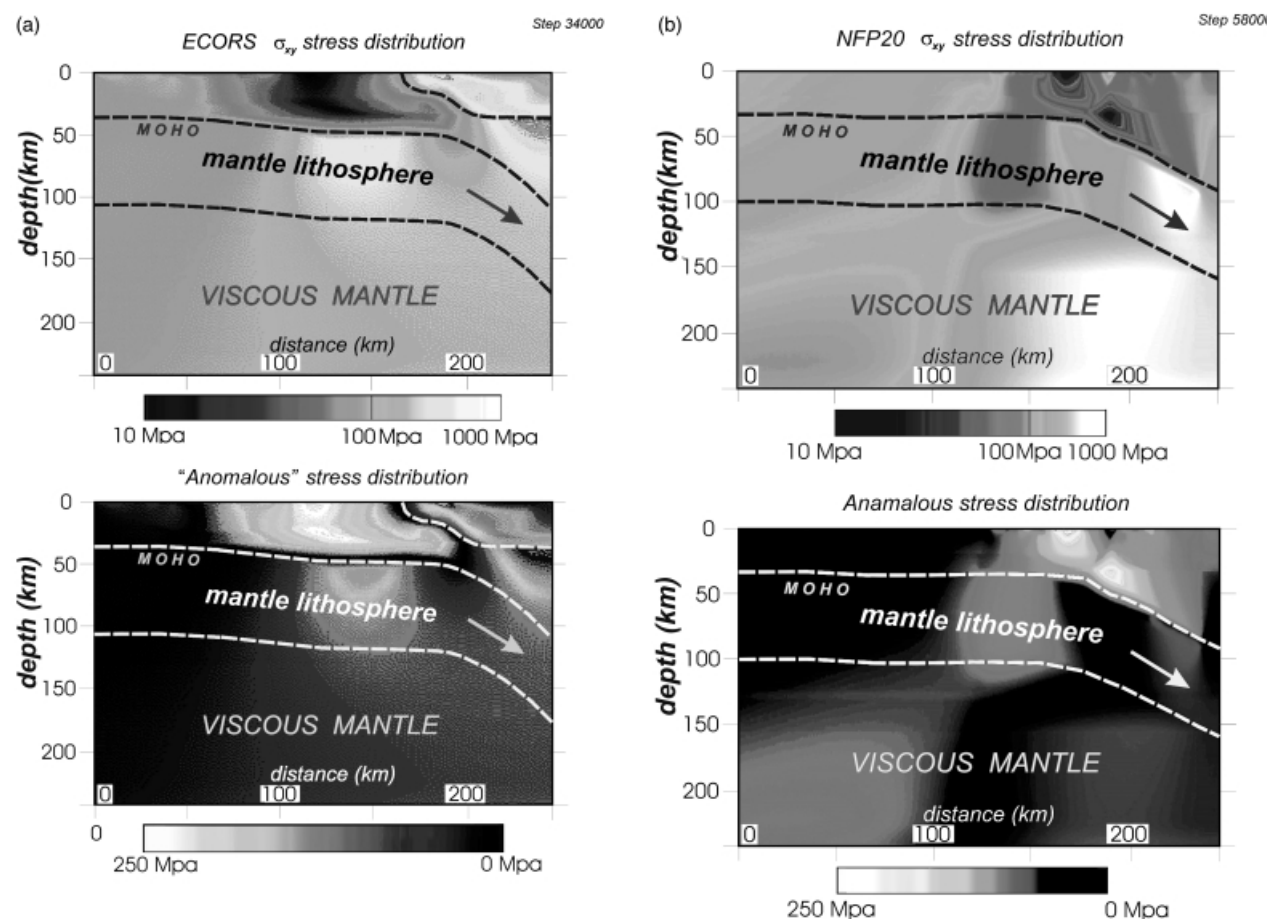


**Fig. 5** Calculated deviatoric shear stress distributions. (a) ECORS profile. Top, deviatoric shear stress distribution; bottom, anomalous stress distribution showing the difference between the elastic (maximum possible stress) and the inelastic stress (limited by yielding limits). Large differences correspond to potentially unstable zones. (b) NFP20 profile. Top, shear stress distribution; bottom, anomalous stress distribution.

density structure is linked to lithology and rheology structure: weak sediments are lighter than stronger granites, granites are weaker and lighter than mafic granulites and so on. Low-density rocks (up to  $2700 \text{ kg m}^{-3}$ ) can be presented by weak quartz-dominated compositions, denser rocks correspond to stronger basic compositions, and the properties of very dense rocks ( $3300 \text{ kg m}^{-3}$ ) should be close to those of mantle olivine. Some additional data such as seismic reflectivity and electric resistivity anomalies provide additional constraints on the rheological behaviour and composition.

The elastic mechanical models of the lithosphere are most stable ones. Yet the rocks can be elastic only when slightly or rapidly deformed. At larger strain and geological strain rates the rocks are brittle or ductile: depending on the local strain velocity and strain

rate field, inelastic zones may evolve rapidly. Their (model-predicted) locations will indicate problematic 'spots' where the input geological structure may be unstable and thus likely to be revised. By modifying the input structure and then repeating thermo-mechanical tests, we 'converge' to a physically consistent geological model compatible with the ensemble of available data.

### Results and discussion

We tested various density and lithology structures previously inferred from the ECORS and NFP20 profiles (Fig. 2). To derive the rheological properties of these structures, we used known relationships between different lithologies and densities (Turcotte and Schubert, 1982; Gao *et al.*, 1998): weak sediment rheology (zero cohesion in the brittle

part) is attributed to the rocks lighter than  $2300 \text{ kg m}^{-3}$ ; quartz-dominated rheology (20 MPa cohesion for the brittle part) is assigned to the density interval between 2300 and  $2750 \text{ kg m}^{-3}$ ; diabase/mafic granulite rheology is used between 2750 and  $2950 \text{ kg m}^{-3}$ ; and olivine rheology is assumed for the rocks denser than  $2950 \text{ kg m}^{-3}$  (Table 1, Fig. 4). Whatever the lithology, denser rocks are stronger.

The numerical results are presented in Figs 5 and 6. For each input configuration from Fig. 2, we calculated residuals between the actual stress and the elastic (maximal) stress. The results shown in Figs 5 and 6 correspond to the input configuration II from Fig. 2(b). In these figures, the areas of high stress difference (i.e. comparable to lithostatic pressure) correspond to important inelastic (plastic or viscous) deformation. Their geometry is unstable and

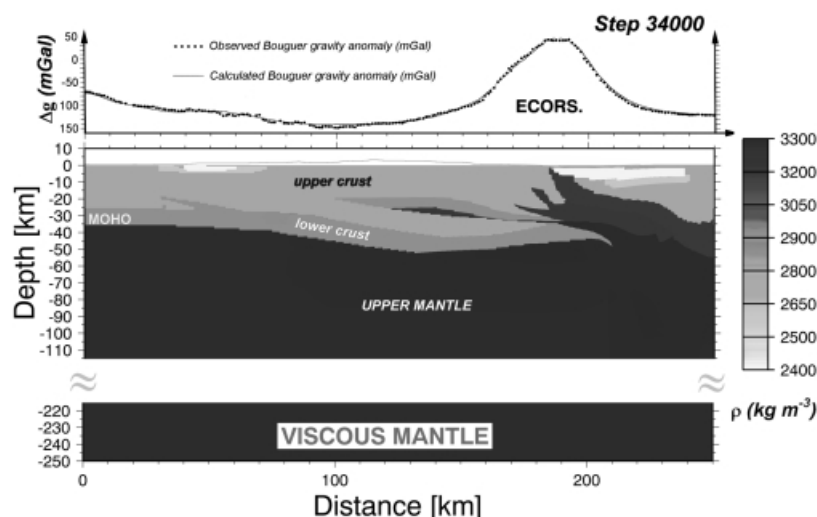


**Fig. 6** Example of ECORS profile. Suggested mechanically, seismic-and gravity-consistent density/lithology structure. Topm observed and calculated Bouguer gravity anomalies.

cannot be preserved on long timescales. For example, the density structure for ECORS profile suggested in Bayer *et al.* (1989) (Fig. 2b, II) is mechanically unstable because the inferred sharp crustal features reach the yield state. For this configuration, the local strain rates reach  $10^{-13} \text{ s}^{-1}$ , whereas the local stresses tend to modify the initial geometry. In particular, the inferred geometry of the 'crocodile' structures on the WNW side of the Alpine part of the ECORS profile, as well as that of the Ivrea body, are mechanically unstable, so that the computed local uplift rates reach unrealistic values of 8–15 mm  $\text{yr}^{-1}$  in the Ivrea body region. Our computations suggest a different, more stable and physically consistent geometry (Fig. 6), which is also entirely compatible with the initial seismic, gravity and geodesy data (vertical surface rates  $< 1 \text{ mm yr}^{-1}$ ) (Fig. 6). For this reason, it presents a better approximation to the real crustal and lithospheric structure. Configuration III from Fig. 2(b) and the density/lithology profile inferred for NFP20 profile (Marchant and Stampfli, 1997) generate smaller stress/strain anomalies than that for the tested parts of structures II and I (Fig. 2b) previously suggested for the ECORS profile. In particular, the tested structure of the NFP20 profile (Fig. 2c) almost entirely satisfies the requirements of mechanical equilibrium, with the exception of a small area corresponding to the upper part of the Ivrea body. Thus the inferred

geometry is probably much closer to the real one. Another, quite puzzling result suggests that the deep crustal structure along the central Alpine ECORS profile is self-sufficient for initialization and continuation of subduction at the current rate. Even if the initial cause for subduction was different (slab pull, convection, etc.), it turns out that the geometries of the colliding plates were readjusted during collision, and now subduction may continue without any additional forces.

### Conclusions

Our model exploits the interdependence of a larger variety of geophysical data (gravity, seismic, geodetic, thermal, stratigraphy, etc.) than the more commonly used solely geophysical tools, thus allowing for more realistic and more self-consistent geological models, i.e. for 'mechanical' validation of deep structures inferred from multidisciplinary data. It helps to select the most physically consistent structures from possible geometries, to trace out problematic spots in the data, as well as to verify more general geodynamic models. In particular, we have shown, using the example of well-studied Alpine cross-sections, that several critical features in the presently inferred deep crustal geometries may be mechanically invalid. For the ECORS profile, it concerns the geometry of the Ivrea body and that of the doubled crust (also called 'crocodile' structures). The deep

structure previously inferred for the NFP20 profile is closer to the mechanical equilibrium, but also may have some problematic features in the Ivrea body zone. The proposed new 'mechanically balanced' cross-sections not only satisfy the previously used data, but are also mechanically stable and consistent with thermal and geodetic data. Nevertheless, because of the uncertainties in the parameters and ambiguities in the data, there is no warranty that the mechanically consistent geological models are the true ones. However, we can be confident that they are much closer to the reality than the scenarios inferred from seismic, gravity or geological data only. The proposed method may have versatile applications for multidisciplinary studies of zones of wide geodynamic interest.

### Acknowledgements

We thank M. Diament and two anonymous reviewers for their highly constructive comments. GeoFrance 3D contribution # 59. BRGM contribution 99168.

### References

- Bayer, R., Carozzo, M.T., Lanza, R., Miletto, M. and Rey, D., 1989. Gravity modelling along the ECORS-CROP vertical seismic reflection profile through the Western Alps. *Tectonophysics*, **162**, 203–218.
- Bernoulli, D., 1981. Ancient continental margins of the Tethyan ocean. Geology of passive continental margins. *Am. Ass. Petrol. Geol., Educ. Course*, **19**, 1–36.
- Bois, C., 1987. Contribution of deep seismic profiling to the knowledge of the lower crust in France and neighboring areas. *Tectonophysics*, **145**, 246–253.
- Brace, W.F. and Kohlstedt, D.L., 1980. Limits on lithospheric stress imposed by laboratory experiments. *J. Geophys. Res.*, **85**, 6248–6252.
- Burov, E.B., Jaupart, C. and Mareschal, J.C., 1998. Large-scale crustal heterogeneities and lithospheric strength in cratons. *Earth Planet. Sci. Lett.*, **164**, 205–219.
- Burov, E.B., Lobkovsky, L.I., Cloetingh, S. and Nikishin, A.M., 1993. Continental lithosphere folding in Central Asia (part 2), constraints from gravity topography. *Tectonophysics*, **226**, 73–87.
- Cundall, P.A., 1989. Numerical experiments on localization in frictional materials. *Ingenieur-Archiv*, **59**, 148–159.
- Damotte, B., Nicolich, R., Cazes, M. and Guellec, S., 1990. Mise en oeuvre, traitement et présentation du profil Plaine du Pô-Massif Central. *Mém. Soc. Géol. Fr.*, **156**, 55–64.

- ECORS-CROP Deep Seismic Sounding Group, 1989. A new picture of the Moho under the western Alps. *Nature*, **337**, 249–251.
- Frei, W., Heitzmann, P. and Lehner, P., 1990. Swiss NFP20 research program of the deep structure of the Alps. *Mém. Soc. Géol. Fr.*, **156**, 29–46.
- Gao, S., Zhang, B.-B., Jin, Z.-M., Kern, H., Luo, T.-C. and Zhao, Z.-D., 1998. How mafic is the lower continental crust? *Earth Planet. Sci. Lett.*, **161**, 101–117.
- Gerbault, M., Burov, E.B., Poliakov, A. and Dagnieres, M., 1999. Do faults trigger folding in the lithosphere? *Geophys. Res. Lett.*, **26**, 2 271–2 274.
- Marchant, R.H. and Stampfli, G.M., 1997. Crustal and lithospheric structure of the Western Alps. In: *Deep Structure of the Swiss Alps: Results of NFP20* (O.A. Pfiffner *et al.*, eds), 326–337. Birkhauser, Basel.
- Hirn, A., Nadir, S., Thouvenot, F. *et al.*, 1989. Mapping the Moho of the Western Alps by wide-angle reflection seismics. *Tectonophysics*, **162**, 193–202.
- Kirby, S.H. and Kronenberg, A.K., 1987. Rheology of the lithosphere: Selected topics. *Rev. Geophys.*, **25**, 1219–1244.
- Kissling, E., 1993. Deep structure of the Alps – what do we really know? *Phys. Earth Planet. Int.*, **79**, 87–112.
- Kissling, E. and Spakman, W., 1996. Interpretation of tomographic images of uppermost mantle structure: examples from the Western and Central Alps. *J. Geodynamics*, **21**, 97–111.
- Laubscher, H.P., 1988. Material balance in Alpine orogeny. *Bull. Geol. Soc. Am.*, **100**, 1313–1328.
- Ledru, P. and Groupe de Recherche GéoFrance 3D, 1997. GEOFRANCE 3D: l'imagerie géologique et géophysique 3D du sous-sol de la France. *Mém. Soc. Géol. Fr.*, **172**, 53–71.
- Nicolas, A., Hirn, A., Nicolich, R., Polino, R. and the ECORS-CROP Working Group, 1990. Lithospheric wedging in the Alps inferred from the ECORS-CROP traverse. *Geology*, **18**, 587–590.
- Nicolas, A., 1990. ECORS-CROP traverse and deep structure of the Alps. *Mém. Soc. Géol. Fr.*, **156**, 15–28.
- Pfiffner, O.A., Frei, W., Finck, P. and Valasek, P., 1988. Deep seismic reflection profiling in the Swiss Alps: explosion seismology results for the NFP20 East. *Geology*, **16**, 987–990.
- Poliakov, A.N.B., Cundall, P., Podladchikov, Y. and Laykhovsky, V., 1993. An explicit inertial method for the simulation of viscoelastic flow: An evaluation of elastic effects on diapiric flow in two- and three-layers models. In: *Flow and Creep in the Solar System: Observations, Modeling and Theory, Dynamic Modelling and Flow in the Earth and Planets* (D.B. Stone and S.K. Runcorn, eds), 175–195. Kluwer, Dordrecht.
- Rey, D., Quarta, T., Mouge, P. *et al.*, 1990. Gravity and aeromagnetic maps on the western Alps: contribution to the knowledge on the deep structures along the ECORS-CROP seismic profile. *Mém. Soc. Géol. Fr.*, **156**, 107–122.
- Thouvenot, F., Paul, A., Senechal, G., Hirn, A. and Nicolich, R., 1990. ECORS-CROP wide -angle reflection seismic: constraints on the deep surfaces beneath the Alps. *Mém. Soc. Géol. Fr.*, **156**, 97–106.
- Trümpy, R., 1985. Die plattentektonik und die Alpen. *Vjschr. Natf. Ges. Zürich*, **129**, 47.
- Tsenn, M.C. and Carter, N.L., 1987. Flow properties of continental lithosphere. *Tectonophysics*, **136**, 27–63.
- Turcotte, D.L. and Schubert, G., 1982. *Geodynamics. Applications of Continuum Physics to Geological Problems*. John Wiley, New York.
- Valasek, P., Frei, W., Stäuble, M. and Holloger, K., 1990. Processing of the NFP20 seismic reflection traverses across the Swiss Alps by the ETH-Zürich data processing center. *Mém. Soc. Géol. Fr.*, **156**, 55–64.
- Viallon, P., 1990. Deep Alpine structures and geodynamic evolution: an introduction and outline of a new interpretation. *Mém. Soc. Géol. Fr.*, **156**, 7–14.

*Received 15 March 1999; revised version accepted 23 September 1999*